Spectroscopic Characterization of Cytochrome ba_3, a Terminal Oxidase from *Thermus thermophilus*: Comparison of the a_3/Cu_B Site to That of Bovine Cytochrome aa_3[†]

W. Anthony Oertling,[*,‡,§] Kristene K. Surerus,[‡,∥] Ólöf Einarsdóttir,[‡,⊥] James A. Fee,[‡,#] R. Brian Dyer,[▽] and William H. Woodruff[*,‡]

Inorganic and Structural Chemistry Group (INC-14, Mail Stop C-345) and Chemical Laser Science Group (CLS-4, Mail Stop J-567), Los Alamos National Laboratory, Los Alamos, New Mexico 87545, Department of Chemistry and Biochemistry, Eastern Washington University, Mail Stop 74, Cheney, Washington 99004, and Department of Biology, University of California at San Diego, La Jolla, California 92093-0322

Received October 7, 1993; Revised Manuscript Received January 3, 1994[⊕]

ABSTRACT: Unliganded and cyano derivatives of cytochrome ba_3 from *Thermus thermophilus* have been examined by UV–vis, EPR, and resonance Raman spectroscopies. Species of cytochrome ba_3 investigated include its resting, as-isolated, fully oxidized state, the fully reduced, unliganded enzyme, the one-electron-reduced cyano complex, the three-electron-reduced cyano complex, and the fully reduced cyano complex. Results are compared to those obtained from similar adducts of bovine cytochrome aa_3, in particular, the fully reduced cyano complex. Our objective was to identify structural similarities and differences at the ligand-binding binuclear site of the two enzymes. We observed that the inner core skeletal vibrations of cytochrome a_3 are the same for similar adducts of the bacterial ba_3 and mammalian aa_3, indicating similar spin and iron–porphyrin coordination properties resulting in comparable porphyrin core geometries. On the other hand, many of the vibrational frequencies associated with the formyl and vinyl peripheral substituents, and the outer pyrrole carbon atoms differ between the bovine and bacterial enzymes. Use of ^{57}Fe labeled ba_3 allows identification of two separate νFe–N(His) frequencies displayed by the fully reduced, unliganded cytochrome. These frequencies, occurring at 193 and 209 cm^{-1}, are ascribed to distinct protein conformers, which are best evidenced by the Fe–N(His) vibrations. This result is again in contrast to the bovine enzyme which has been shown by others to display a single Fe–N(His) stretching frequency at 214 cm^{-1}. The low-frequency Fe_{a3}^{2+}–CN^- vibrations of the three-electron and fully reduced cyano complexes of cytochrome ba_3 are identified by using ^{15}N and ^{13}C isotopomers of CN^-. These spectral signatures are identical to those reported earlier for the one-electron-reduced cyanide adduct (cytochrome a_3 reduced), showing that the Fe_{a3}^{2+}–CN^- vibrational frequencies are independent of the redox states of the other three metal centers. Similarly, the Cu_B^{2+} EPR signatures appear similar in both the one-electron- and three-electron-reduced cyanide adducts. On the other hand, the electronic absorption spectra of ferrous a_3–CN^- show systematic red-shifts of the α band as each of the other metal centers is reduced, and other, more subtle, differences in the electronic absorptions of the three-electron-reduced and four-electron-reduced cyanide adducts are revealed in the difference spectra. The relevance of these findings toward explaining the different cyanide binding and redox chemistry described herein and toward establishing the extent of structural analogy between the oxygen binding sites of the two proteins is discussed.

There exists a "superfamily" of heme–copper containing enzymes that serve as the terminal oxidases of the respiratory chains in mitochondria and in many bacteria [cf. Saraste (1990) for review]. These enzymes accept electrons from cytochromes *c* or quinols, catalyze the four-electron reduction of O_2 to H_2O, and couple the free energy of these electron transfer processes to translocation of protons across the membrane. The detailed chemical mechanisms of coupled electron transfer/proton translocation remain obscure. A large body of work indicates that a conserved structural element, unique to these enzymes and consisting of a closely disposed heme/Cu pair, (commonly termed the binuclear site) is the locus of O_2 reduction [cf. Wikström et al. (1981), Malmström (1990), and Chan and Li (1990) for reviews]. Recently, this site has also been implicated in proton pumping [cf. Babcock and Wikström (1992) for review].

It is now generally believed that the functional core of these enzymes is composed of subunit I, which binds the binuclear heme–Cu pair and an additional heme moeity, subunit II (or IIc), which, in the case of cytochrome *c* oxidases, contains the Cu_A binding site or, in the case of quinol oxidases, lacks Cu_A (Mather et al., 1991), and subunit III, for which a function remains obscure (Puettner et al., 1985). Purified enzymes from eukaryotic cells possess a number of ancillary subunits,

[†] This research was supported by National Institutes of Health Grants DK36263 (to W.H.W.) and GM35342 (to J.A.F.); Northwest Institute for Advanced Study and EWU Foundation grants (to W.A.O); Institutional Supporting Research Grant X15B (to R.B.D.), and Director's Postdoctoral Fellowships (to Ó.E. and K.K.S.) from LANL; and by USPHS Grant RR02231 (A National Stable Isotope Resource at LANL). Work done at LANL was carried out under the auspices of the U.S. Department of Energy.

[*] Author to whom correspondence should be addressed.

[‡] INC-14, Los Alamos National Laboratory.

[§] Present address: Department of Chemistry and Biochemistry, Eastern Washington University, Mail Stop 74, Cheney, WA 99004.

[∥] Present address: Department of Chemistry, University of Wisconsin—Milwaukee, Milwaukee, WI 53201.

[⊥] Present address: Department of Biochemistry, University of California at Santa Cruz, Santa Cruz, CA 95064.

[#] Present address: Department of Biology, University of California at San Diego, La Jolla, CA 92093-0322.

[▽] CLS-4, Los Alamos National Laboratory.

[⊕] Abstract published in *Advance ACS Abstracts,* February 15, 1994.

0006-2960/94/0433-3128$04.50/0

while those purified from prokaryotic cells contain only the three core subunits, and it is not uncommon that subunit III is lost during purification (cf. Ludwig, 1984).

It now appears that hemes A, B, and O (Wu et al., 1990) may be used as cofactors by various members of this enzyme superfamily. For example, the mitochondrial cytochrome aa_3 from bovine heart tissue contains two hemes A, the cytochrome *bo* from *Escherichia coli* utilizes one heme B and one heme O (Puustinen et al., 1991), while the cytochrome ba_3 from *Thermus thermophilus* contains one heme B and one heme A (Zimmerman et al., 1988); there are further variations (Sone et al., 1991). In all cases, these appear to be substitutions of one type of heme for another among structurally similar proteins. As will be noted in this work, the subtle variations in heme type and protein environment, within the context of a generally common structure, support comparative study within this class of enzymes [see however, Musser et al. (1993)].

Of the heme–copper oxidases, the cytochrome aa_3 isolated from bovine heart tissue has been most thoroughly investigated. This protein, however, possesses several properties that complicate its study. These include heterogeneity of isolation products (Brudvig et al., 1981; Baker et al., 1987; Hartzell et al., 1988) and the complex subunit structure mentioned above [cf. Capaldi et al. (1990) for review]. Moreover, the overlap of the electronic spectra of cytochromes *a* and a_3 has always complicated its study by optical methods (Vanneste, 1966), and this is particularly true of resonance Raman spectroscopy. However, early resonance Raman (RR) work on bovine cytochrome aa_3 by the groups of Babcock and Woodruff established that the vibrations of the individual *a* and a_3 chromophores could be distinguished by Raman excitation at various wavelengths within the Soret absorption envelope from 400 to 450 nm (Babcock et al., 1981; Woodruff et al., 1981). Using these techniques, the high-frequency vibrational assignments for the individual *a* and a_3 chromophores were established. A significant contribution was later made by Rousseau and co-workers (Ching et al., 1985; Argade et al., 1986), who, using computer subtractions, arrived at difference spectra which, the authors suggest, represent the resolved individual *a* and a_3 components of the fully reduced unligated, the fully reduced cyanide, and the fully reduced carbon monoxide adducts, as reviewed recently (Babcock, 1988).

Cytochrome ba_3 from *T. thermophilus* was originally described as a single-subunit cytochrome *c* oxidase (Zimmermann et al., 1988). However, recent DNA sequence data from one of our groups suggest that cytochrome ba_3 is a normal, multisubunit member of the heme–copper oxidase family (J. A. Keightley et al., unpublished results). Extensive physical and chemical characterization of this protein reveals that it is a homolog of cytochrome aa_3 in which the low-spin heme A of cytochrome *a* is replaced with heme B while the disposition of the other cofactors remains largely unchanged (Zimmermann et al., 1988; Zimmermann, 1988; Einarsdóttir et al., 1989b; Goldbeck et al., 1992; Surerus et al., 1992), thus, the designation cytochrome ba_3. Although this enzyme exhibits complex behavior, as do all these enzymes, and possesses its own idiosyncrasies, its electronic spectrum allows clear separation of the *b* and a_3 chromophores. Thus, the task of assignments of the vibrational contributions to the individual hemes is greatly facilitated. Here we exploit this property of the hemes in a comparative study of the resonance Raman (RR) spectra of the a_3 site in ba_3 and bovine aa_3.

Much of the present work is focused on the cyano complexes of these enzymes. The oxidized bovine enzyme reacts with cyanide to produce low-spin ferric a_3 which is ferromagnetically coupled to Cu_B^{2+} (Boelens et al., 1983; Li & Palmer, 1993). This electronic structure is thought to arise from a bridged Fe^{3+}–CN^-–Cu^{2+} arrangement in which cyanide is bonded to both metals [Thomson et al., 1981; Kent et al., 1982; Li & Palmer, 1993; cf. Fee et al. (1993) for review]. The reaction of cyanide with oxidized cytochrome ba_3 is quite different. Autoreduction of cytochrome a_3 occurs, and a complex forms having one CN^- bound to low-spin Fe^{2+} and one CN^- bound to Cu_B^{2+}. We and our co-workers (Surerus et al., 1992; Oertling et al., unpublished results) have used a combination of EPR, ENDOR, and RR spectroscopies to yield evidence for a working model of the binuclear site of cyano ba_3.

In this model the ferrous heme A is coordinated to one histidine (the proximal ligand) and one CN^- which does not bridge to the nearby Cu (see discussion below and Oertling et al., unpublished results). Cu_B^{2+} appears to be surrounded by a rigid, tetragonal ligand field resulting from histidine imidazole rings that prevent the axially ligated CN^- (which is weakly coupled magnetically to the Cu^{2+}) from assuming an equatorial coordination position [cf. Surerus et al. (1992) for further discussion]. The geometric constraints placed on the system by these results and the likely close proximity of the two metal centers (Powers et al., 1979; Boelens et al., 1984; Scott et al., 1986; George et al., 1993) dictate that the arrangement of the HisN–Fe–CN and Cu–CN axes are close to parallel, possibly colinear, and that the heme plane and the equatorial plane of the Cu_B complex are also approximately parallel.

It is of interest to determine the general applicability of this model to the ligand binding sites, i.e., the heme a_3/Cu_B binuclear cofactors, of other members of the heme–copper oxidase family. In the present study we compare the structural properties of the binuclear sites of *Thermus* ba_3 and bovine aa_3. Our approach uses UV–vis, EPR, and RR spectroscopies to establish the spin, redox, and coordination states of the metal centers of several different ba_3 derivatives.

EXPERIMENTAL PROCEDURES

Cytochrome ba_3 was isolated from the plasma membrane of *T. thermophilus*, as described elsewhere (Zimmerman, 1988). All ba_3 samples were prepared in 0.1 M phosphate, 0.1% lauryl maltoside buffer at pH 7.4. The concentration of enzyme was determined by UV–visible measurements using reduced minus oxidized $\Delta\epsilon_{613-658} = 6.34\ mM^{-1}\ cm^{-1}$. The one-electron-reduced cyanide complex was prepared by incubation with 10–100-fold excess KCN at room temperature. The incubation time required for complete complexation was preparation dependent ranging from 0.5 h for freshly purified protein to 5–7 days for protein stored a −20 °C for 1 year. After degassing by several pump/flush cycles with moist Ar gas on a vacuum line, reductions were carried out in anaerobic cuvettes or NMR tubes fitted with septa caps through which additions of a buffered solution of sodium dithionite were made. Addition of cyanide to the resting enzyme results in a Fe_{a3}^{2+}–CN^- complex (hence abbreviated a_3^{2+}–CN^-) but leaves all of the other three metal centers oxidized; hence the overall redox state of the enzyme is one-electron reduced. Recent evidence has shown the presence of additional metal centers present in bovine cytochrome oxidase (Einarsdóttir et al., 1988). As these have not been confirmed in ba_3 and as their function in aa_3 is not established, we consider only the traditional four metals in this work. Addition of sodium dithionite to this one-electron-reduced cyanide complex results

in a three-electron-reduced complex in which Cu_B remains cupric but all other metal centers are reduced (see below). Addition of dithionite to the resting enzyme *first*, followed by cyanide, results in a fully (four-electron) reduced cyano complex. In unligated, dithionite-reduced samples at low concentrations, 15 μM or less, upon addition of a 300-fold excess of KCN, an intense absorption band appeared instantaneously at 590 nm and was taken to indicate fast binding of cyanide to the reduced cytochrome a_3. This was confirmed by RR measurement of the Fe–CN stretching and bending vibrations. $K^{13}C^{15}N$ was purchased from Isotec and $KC^{15}N$ from Stohler Isotope Chemicals, and $K^{13}CN$ was supplied by the Stable Isotope Resource of Los Alamos.

All sample preparations were monitored by UV–visible absorption spectra recorded on a Cary-14 (with OLIS upgrade) or a Beckman instrument. RR spectra using 413.1-nm excitation were recorded on a Spex 1403 monochromator with PMT detection while all others were measured with a Spex 1877 Triplemate outfitted with a Photometrix CCD detector cooled by liquid nitrogen. The latter system was necessary to detect the weak FeCN Raman vibrations of the cyanide adducts. Samples at concentrations of 70–300 μM in spinning NMR tubes or cooled, anaerobic cuvettes were illuminated and Raman scattering collected using a 135° back-scattering geometry. Raman spectra of samples at 15 μM in anaerobic cuvettes were measured using a 90° scattering geometry. Laser light at 413.1 nm was provided by a Spectra Physics model 171 krypton ion laser, and tunable excitation from 418–445 nm was obtained from Stilbene dye in a Coherent model 599 dye laser pumped by a Spectra Physics model 2045 argon ion laser. Optical absorption spectra of all samples were checked before and after the Raman measurements and confirmed sample integrity in all cases. EPR spectra were recorded with an IBM EPR 200D fitted with a continuous flow cryostat.

RESULTS

In order to establish the iron redox level and coordination sphere in cytochromes *b* and a_3 of the various complexes studied, we first examined UV–visible spectra, EPR spectra, and Raman data in the 1300–1700-cm^{-1} range. The vibrational frequencies of the porphyrin in this spectral region are known to be sensitive to the spin state and ligation number of the metal in both heme proteins and model compounds. This is by virtue of the dependence of these frequencies on the exact geometric conformation the macrocycle assumes in response to the effective size of the metal and the constraints arising from the axial ligands. Due to the overlap of the iron d_{xz} and d_{yz} and the porphyrin π^* orbitals, the vibrational force field of the porphyrin is affected by the oxidation state of the iron; hence, there are characteristic frequencies for ferrous and ferric porphyrins.

Figures 1 and 2 display UV–visible spectra, and Table 1 collects absorbance maxima of the ba_3 derivatives examined in this work. Figures 3 and 4 contain RR spectra of the resting and fully reduced, unligated enzyme, respectively. The polarized spectra and multiple excitation wavelengths used allow resolution of the contributions from the individual hemes. Figures 5–7 show data from cyanide derivatives. The RR spectra presented in Figures 5 and 7 reflect the redox and coordination state of cytochromes *b* and a_3 and the EPR measurements of Figure 6 monitor the copper centers of these cyanide complexes. Vibrational assignments for cytochrome *b* are collected in Table 2, and vibrational assignments for cytochrome a_3 appear in Table 3. The normal mode descriptions and numbering scheme were originally proposed by

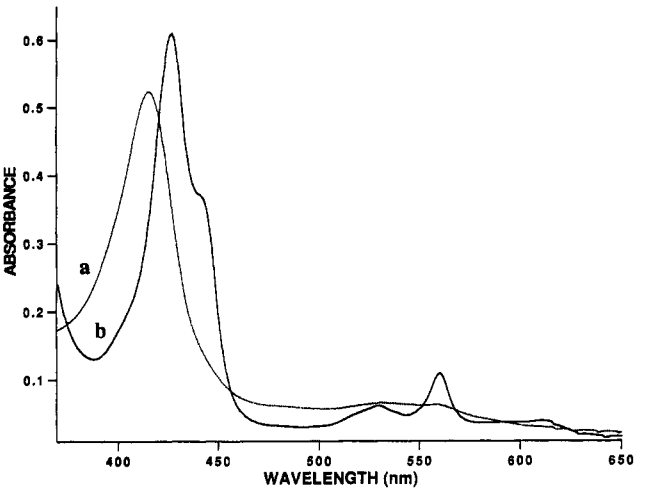

FIGURE 1: UV–visible absorbance spectra of the (a) resting (···) and (b) fully reduced, unligated (—) enzyme.

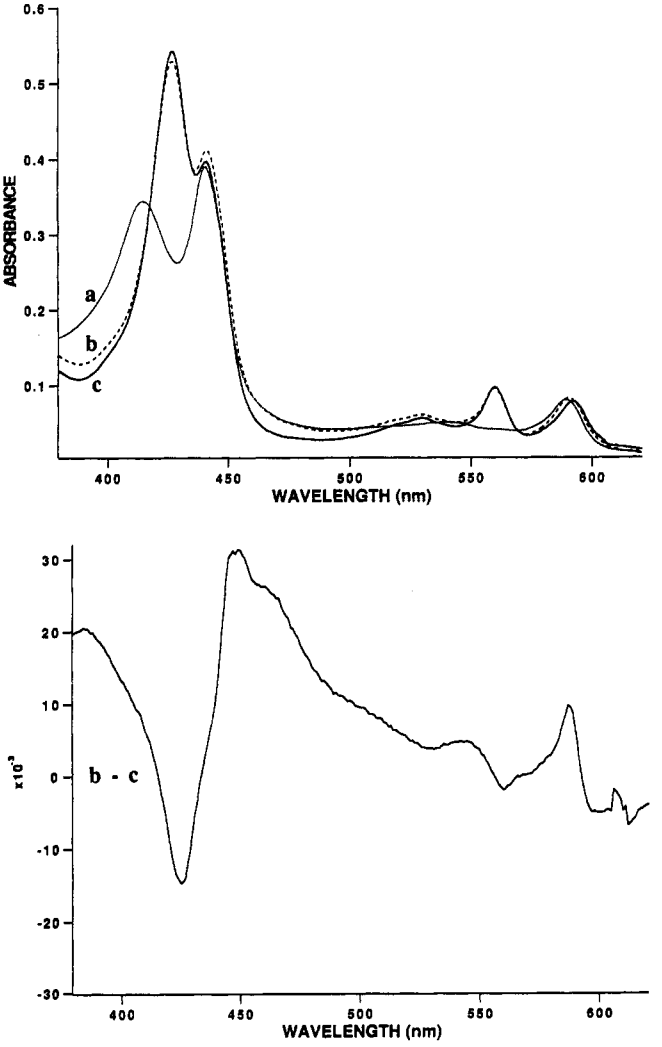

FIGURE 2: (a) One-electron-reduced cyanide (···), (b) three-electron-reduced cyanide (- - -), and (c) four-electron reduced cyanide (—) derivatives of cytochrome ba_3 oxidase. (b – c) Difference spectrum. (c) Formed by reducing the protein prior to addition of cyanide. Sample concentrations were approximately 15 μM. Details of preparations appear under Experimental Procedures.

Abe et al. (1978). The focus of the present work is on the a_3 vibrational frequencies. For comparison, therefore, we list previously reported values for the bovine enzyme (Table 3) and relevant Fe–porphyrin model compounds (Table 4).

Table 1: UV–Visible Absorption Maxima (nm) for Individual *b* and a_3 Chromophores of Cytochrome ba_3

	a_3		*b*		
	Soret	α	Soret	α	β
resting	~418	diffuse	~415	diffuse	diffuse
fully reduced, unligated	442	612	427	530	560
one-electron-reduced, CN^-	440	589	415	diffuse	diffuse
three-electron-reduced, CN^-	441	591	427	530	560
four-electron-reduced, CN^-	441[a]	592	427	530[a]	560[a]

[a] These absorptions exhibit small (<1 nm) shifts compared to those of the three-electron-reduced adduct as discussed in the text.

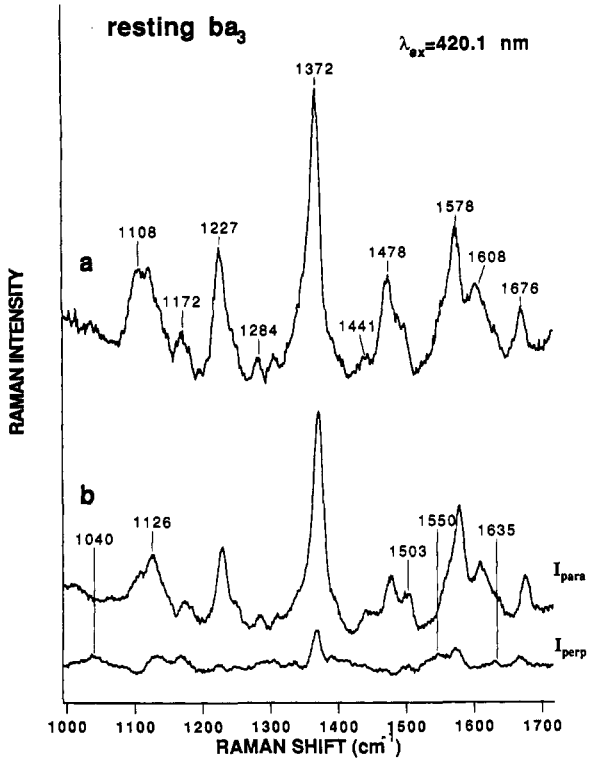

FIGURE 3: High-frequency RR spectra of resting cytochrome ba_3 oxidase. Laser power at 420.1 nm was 15 mW. The sample (150 μM) was in a spinning NMR tube at 10 °C, with 135° back-scattering geometry. Total accumulation time for each spectrum was 20 min; parallel and perpendicular scattering runs were repeated three times total. All were measured using CCD detection and a 1200 grooves/mm grating.

Resting Enzyme. The spectral resolution of the two hemes in the Soret region is poorest for the resting enzyme. However, Einarsdóttir et al. (1989a) showed that the RR spectra obtained with 413.1-nm laser excitation of resting ba_3 and that of the oxidized form of cytochrome b_5 from rat liver could be subtracted to obtain those spectral contributions arising from the heme a_3 chromophore of ba_3. These results are strongly supported by RR spectra of resting cytochrome ba_3 presented in Figure 3. We find that the most intense features of the scattering obtained using excitation at 420.1 nm (Figure 3a) arise from a_3, and this spectrum is comparable to the difference spectrum reported earlier. In agreement with Einarsdóttir et al. (1989a), we assign the two most intense features at 1372 and 1578 cm^{-1} to overlapping bands of each of the two heme groups. However, the band at 1478 cm^{-1} is more clearly apparent at this excitation wavelength than in the earlier work, and this frequency is significant to the Fe_{a3} coordination assignment. From the reported frequencies, Fe_{a3} in the resting bacterial enzyme is clearly a ferric, high-spin species, consistent with previous Mössbauer studies (Zimmerman et al., 1988). Einarsdóttir et al. (1989a) noted that the 1578-cm^{-1} ν_2 value

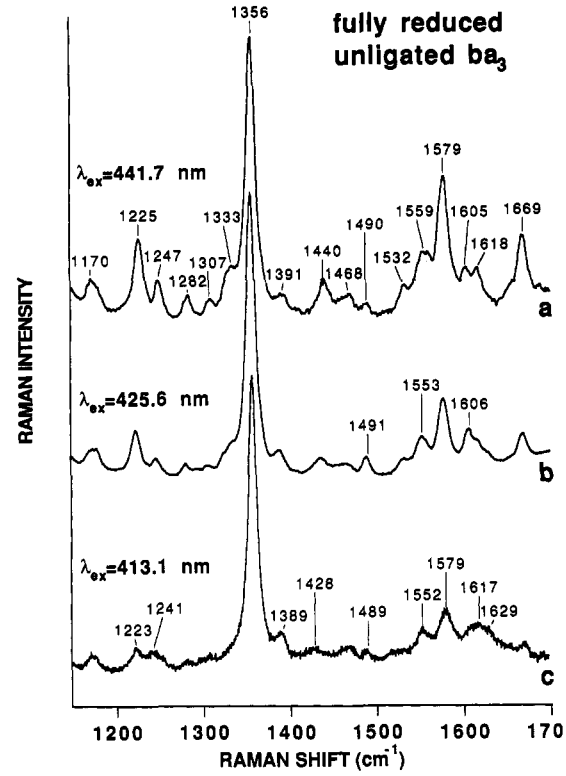

FIGURE 4: High-frequency RR spectra of fully reduced, unligated cytochrome ba_3 oxidase. Spectra were collected using 135° back-scattering geometry. (a and b) Laser power at 441.7 and 425.6 nm was 45 mW. The sample (120 μM) was in an anaerobic quartz cuvette at 10 °C. Total accumulation time for spectra a and b was 20 min using CCD detection and a 1200 grooves/mm grating. (c) The sample was 70 μM in a sealed, spinning NMR tube at 25 °C. Laser power at 413.1nm was 15 mW; spectrum represents 10 scans on a Spex 1403 with PMT detection.

(Table 3) is higher than that of the corresponding frequency in bovine aa_3 (1572 cm^{-1}, see Table 3) and suggested that the porphyrin A macrocycle of cytochrome a_3 is more contracted in ba_3 than in aa_3. Our present analysis shows that this may not be so. It is most likely that such a contracted core would arise from a five-coordinate rather than a six-coordinate high-spin (6chs) ferric complex; thus the suggestion of these authors is germane to the coordination assignment of Fe_{a3}. Although the 1578 cm^{-1} ν_2 frequency may be taken to suggest a contracted core size characteristic of a five-coordinate complex, the 1478 ν_3 and 1608 cm^{-1} ν_{10} values clearly establish that Fe_{a3} is predominantly six- rather than five-coordinate, at room temperature. These predictions are based on the known frequency–structure correlations (Spaulding et al., 1976; Callahan & Babcock, 1981; Choi et al., 1982) and arise from the typical sizes that the five- and six-coordinate high-spin (6chs) Fe^{3+} ions assume in the porphyrin complexes. Because the 1478- and 1608-cm^{-1} vibrations are stretching motions of the inter-pyrrole methine bridges, their frequency dependence on porphyrin center-to-nitrogen distance (or "core size") is stronger than that of ν_2, which is a pyrrole b-carbon stretch. Furthermore, the ν_2 frequency can potentially be affected by the peripheral groups on the porphyrin, which may impose an effect contrary to the expected core-size dependence. For these reasons the Fe_{a3} coordination number is best predicted from the ν_3 and ν_{10} frequencies to be six, and the resulting core size is most likely that typical of the 6chs configuration. Below, we offer an alternative explanation to that of Einarsdóttir et al. (1989a) for the elevated ν_2 frequency in resting ba_3.

Although the spectrum in Figure 3a is dominated by contributions from a_3, features attributable to *b* can be

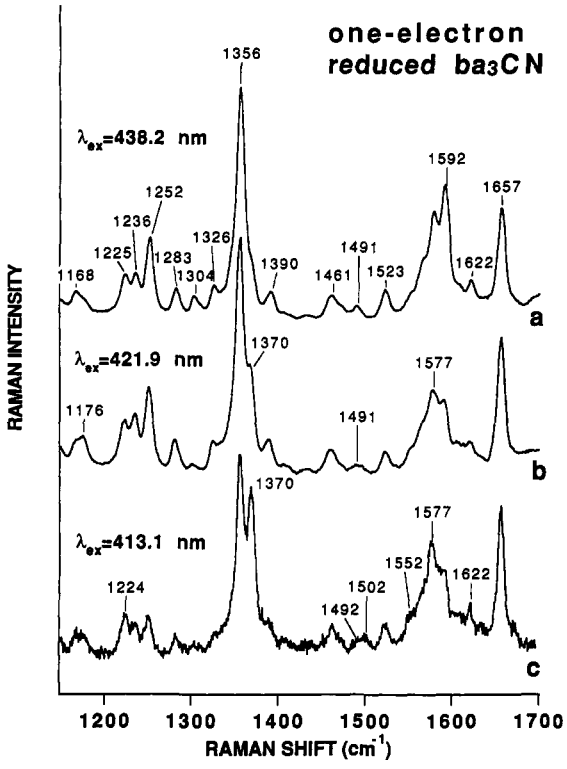

FIGURE 5: High-frequency RR spectra of the one-electron-reduced cyanide derivative of cytochrome ba_3 oxidase. Samples (80 μM) were in spinning NMR tubes, at 10 (a and b) or 25 °C (c), with 135° back-scattering geometry. (a) Laser power at 438.2 nm was 25 mW, with a 30-min accumulation using CCD detection and a 1200 grooves/mm grating. (b) Laser power at 421.9 nm was 15 mW, with a 20-min accumulation as in spectrum a. (c) Laser power at 413.1 nm was 15 mW, with 10 scans.

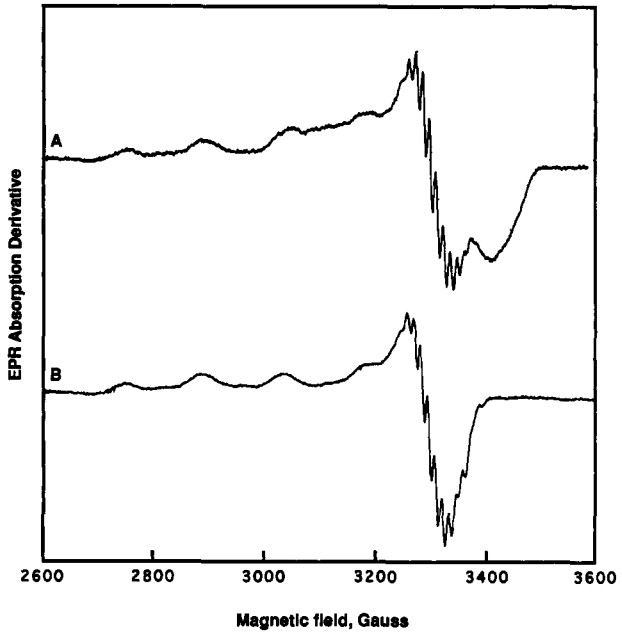

FIGURE 6: EPR spectra of the (a) one-electron-reduced cyanide and (b) three-electron-reduced cyanide complexes of cytochrome ba_3. Conditions: (a) 80 μM sample, 50 K, 5 mW of microwave power, 5 G modulation amplitude at 100 kHz, and 9.42 GHz microwave frequency. (b) Conditions were the same, but the field modulation was 10 G.

identified in Figure 3b which shows Raman scattering polarized parallel and perpendicular to the incident beam. A shoulder on the cytochrome a_3 band at 1478 cm^{-1} occurs at 1503 cm^{-1} (ν_3, polarized), as viewed in the parallel scattering,

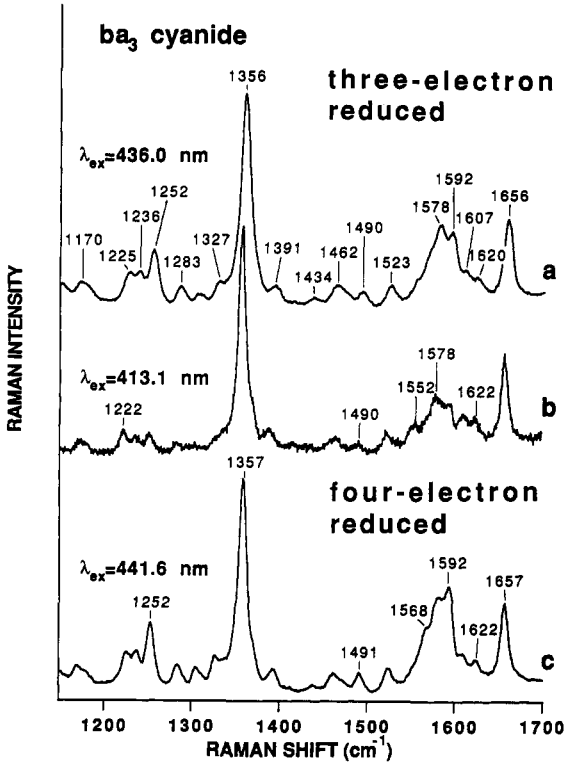

FIGURE 7: High-frequency RR spectra of the three- and four-electron-reduced cyanide derivatives of cytochrome ba_3 oxidase. Samples (80 μM) were in spinning NMR tubes, at 10 (a and c) or 25 °C (b), with 135° back-scattering geometry. (a) Laser power at 436.0 nm was 20 mW, with a 20-min accumulation using CCD detection and a 1200 grooves/mm grating. (b) Laser power at 413.1 nm was 15 mW, with 10 scans. (c) Laser power at 441.6 nm was 30 mW, with a 20-min accumulation as in spectrum a.

Table 2: RR Frequencies (cm^{-1}) for Six-Coordinate Low-Spin Cytochrome *b* in ba_3 Derivatives

assignment[a]	resting b^{3+}	fully reduced unligated b^{2+}	one-electron-reduced cyanide b^{3+}	three-electron-reduced cyanide b^{2+}
$\nu_{C=C}$(vinyl)	1620	1617	1622	1622
ν_{10}	1635	1629		
$\nu_2(C_bC_b)$	1578	1579	1577	1578
$\nu_{11}(C_bC_b)$	1550	1552	1552	1552
ν_3	1503	1489	1502	1490
δ_s =CH$_2$(1)		1428		
ν_{20}, ν_{29}		1389		
ν_4	1372	1356	1370	1356

[a] Normal mode descriptions are from Abe et al. (1978), Choi et al. (1982), and Li et al. (1990). Vibrational frequencies and assignments are in agreement with RR work cytochrome b_{559} by Babcock et al. (1984).

and weak, depolarized features are apparent in the perpendicular scattering component at 1550 (ν_{11}) and 1635 cm^{-1} (ν_{10}). The depolarization ratios ($I_\perp/I_\parallel$) of these three features are consistent with assignment as vibrations of cytochrome *b*, which, unlike heme A, displays effective D_{4h} symmetry with the attendant consequences for the polarization of resonance Raman scattering (Woodruff et al., 1983). Similarly, the smaller depolarization ratios of the 1478- and 1608-cm^{-1} features are consistent with their assignments to ν_3 and ν_{10} of cytochrome a_3. In the effective D_{2h} symmetry expected for an A-type heme, both of these vibrations correlate to totally symmetric modes and are expected to be polarized (Wilson et al., 1955). The vibrational frequencies for cytochrome *b* in Table 2 are in agreement with earlier analysis of iron protoporphyrin model compound spectra (Choi et al., 1982) and RR spectra of plant cytochrome b_{559} (Babcock et al.,

Table 3: RR Frequencies (cm^{-1}) for Cytochrome a_3 in ba_3 and aa_3 Oxidases

	ba_3			aa_3		
assignment[a]	resting 6chs a_3^{3+}	fully reduced unligated 5chs a_3^{2+}	cyanide 6cls a_3^{2+}	resting[b] 6chs a_3^{3+}	fully[c] reduced unligated 5chs a_3^{2+}	fully[c] reduced cyanide 6cls a_3^{2+}
$\nu_{C=O}$(formyl)	1676	1669[d]	1657* [d]	1676	1665	1644
$\nu_{C=C}$(vinyl)		1618	1622		1622	1625
ν_{10}	1608	1605		1610	1607	
ν_{37}			1607			1604
$\nu_2(C_bC_b)$	1578*	1579	1592*	1572	1579	1580*
$\nu_{38}(C_bC_b)$		1559*	1568		1565	1561
$\nu_{11}(C_bC_b)$		1532	1523		1518*	1520
ν_3	1478		1491	1478	1473	1491
δ_s=CH_2(1)	1441	1440	1435		1435*	
ν_{20},ν_{29}		1391	1391		1389	1391
ν_4	1372	1356	1356	1373	1355	1357
δ_s=CH_2(2)	1343	1333	1327		1327	1328
ν_{21}, δ(CH=)	1308	1307	1304		1304	1304
ν_{42}	1284	1282	1283		1285	1285
$\nu_5(C_bS) + \nu_9(\delta C_bS)$[e]		1247	1252		1247	1255
$\nu_{13}(\delta C_mH)$[e]	1227	1225	1225		1225	1224
νC_b–CHO[e]	1227	1225	1236		1225	1236
ν_{30}	1172	1170	1169			

[a] Normal mode descriptions are from Abe et al. (1978), Choi et al. (1983), and Li et al. (1990). [b] Taken from Carter et al. (1981), Woodruff et al. (1981), Schoonover et al. (1988), and Babcock and Callahan (1983). [c] Taken from Callahan and Babcock (1983) and Ching et al. (1985). [d] An asterisk indicates that the frequency differs significantly (>4 cm^{-1}) from the other oxidase and from the model compound. Underlining indicates that the frequencies of both oxidases are similar and differ significantly (>4 cm^{-1}) from that of the model compound. [e] Assignments in this region are uncertain as are correlations to the model compound results in Table 2.

Table 4: RR Frequencies (cm^{-1}) for Heme A Model Compounds

assignment[a]	$(DMSO)_2Fe^{3+}PA$[b] 6chs	$(2MI)Fe^{2+}PA$[c] 5chs	$(NMI)_2Fe^{2+}PA$[d] 6cls
$\nu_{C=O}$(formyl)	1670[e]	1660	1644[f]
$\nu_{C=C}$(vinyl)	1622	1624	1622
ν_{10}	1611	1607	1615
ν_{37}			~1605
$\nu_2(C_bC_b)$	1570	1578	1587[f]
$\nu_{38}(C_bC_b)$	1560	1564	1565[f]
			1545
$\nu_{11}(C_bC_b)$	1522	1533	1515[f]
ν_3	1480	1473	1493
δ_s=CH_2(1)	1442	1443	
ν_{20}, ν_{29}		1395	1391
ν_4	1371	1357	1359
δ_s=CH_2(2)	1336	1332	1332
ν_{21}, δ(CH=)	1313	1313	1308
ν_{42}	1284	1283	1280
$\nu_5(C_bS) + \nu_9(\delta C_bS)$		1249	1248[f]
$\nu_{31}(\delta C_mH)$		1230	1229
νC_b–CHO	1230	1230	1229[f]
ν_{30}	1175	1174	1167

[a] Normal mode descriptions are from Abe et al. (1978), Choi et al. (1983), and Li et al. (1990). [b] Taken from Callahan and Babcock (1981) and Choi et al. (1983). [c] Taken from Van Steelandt-Frentrup et al. (1981) and Choi et al. (1983). The solvents used were CH_2Cl_2 and 2% Brij, respectively. [d] Taken from Van Steelandt-Frentrup et al. (1981), Babcock and Callahan (1983), and Choi et al. (1983). The solvents were CH_2Cl_2 and DMSO. [e] There is a 6-cm^{-1} spread in the reported frequencies. This is an average. [f] These frequencies show significant solvent dependence. These values are from samples in CH_2Cl_2 or DMSO solvents.

1985). These results confirm the ferric, six-coordinate low-spin (6cls) character of the *b* component of resting cytochrome ba_3 originally proposed from Mössbauer spectra (Zimmerman et al., 1988).

Fully Reduced Unligated Enzyme. Addition of excess sodium dithionite to the resting enzyme results in reduction of all four metal centers, i.e., a four-electron reduction of the protein. High-frequency RR spectra of this derivative obtained using 441.7-, 425.6-, and 413.1-nm excitation are shown in Figure 4. Because the Soret absorptions of the reduced hemes are more resolved than in the resting state (see Figure 1; Table 1), the individual spectral contributions can readily be ascertained by varying the excitation wavelength. As expected, the 441.7-nm spectrum is dominated by contributions from a_3, and the majority of vibrations are assigned in Table 3. These vibrational frequencies firmly establish the presence of a ferrous, five-coordinate high-spin (5chs) heme a_3 in this derivative at 10 °C. Some contributions from heme *b* are present (e.g., the weak feature at 1490 cm^{-1}), and these become more evident as the excitation is shifted toward the blue. Indeed, the spectrum obtained with 413.1-nm excitation is predominantly scattering from cytochrome *b*, and the features indicated in Figure 4c and their assignments in Table 2 firmly establish the ferrous, six-coordinate low-spin (6cls) configuration, thus corroborating the assignment from the Mössbauer data (Zimmerman et al., 1988). There is considerable correspondence of the vibrational frequencies of the two hemes in the fully reduced, unligated derivative. In particular the dominant ν_4 feature at 1356 cm^{-1}, common to all ferrous hemes, occurs in both. As mentioned above, the ν_2 feature is conveniently used to establish the spin state of A type hemes because of its large relative intensity in Soret RR spectra. That is, a low-spin heme A complex will display a ν_2 frequency quite distinct from that of a high-spin complex (see Table 4). This vibrational frequency coincidentally overlaps at 1579 cm^{-1} in the 6cls heme *b* and the 5chs heme a_3 moieties of cytochrome ba_3, however, because the peripheral substituents of the two porphyrins differ. Thus, superficially, there appears little spectral change in the RR spectra of Figure 4 as the excitation wavelength is varied toward the blue. Nonetheless, the reduced intensity in the spectrum obtained with the violet excitation (Figure 4c) of the 1669-, 1532-, and 1440-cm^{-1} features clearly characteristic of an A-type heme (see Tables 3 and 4 for vibrational assignments) supports our analysis.

One-Electron-Reduced Cyanide Complex (Fe_{a3}^{2+}–CN^-, Cu_B^{2+}–CN^-, Fe_a^{3+}, Cu_A^{2+}). Addition of excess cyanide to native cytochrome ba_3 results in a novel mixed valence complex containing an oxidized Fe_b/Cu_A cofactor and a Fe_{a3}/Cu_B cofactor reduced by one electron. This reaction is not known to occur in other heme–copper oxidases. We have studied this complex extensively by UV–vis, EPR, ENDOR, and RR spectroscopies in conjunction with permutations of isotopically labeled cyanide (Surerus et al., 1992). The complex displays

clearly resolved Soret electronic absorptions (Figure 2a), and, like the fully reduced unligated derivative, affords good opportunity for selective RR excitation. Figure 5 shows RR spectra obtained with a variety of excitation wavelengths in the Soret region. The ν_4 mode, or "oxidation-state marker", observed at 1356 cm^{-1} using 438.2-nm excitation is typical of a ferrous heme and provides convincing evidence that autoreduction of heme a_3 occurs upon addition of cyanide to the native enzyme. As the Raman excitation is shifted toward the blue, stronger resonance conditions are established with the protoheme chromophore and the ν_4 vibration, visible at 1370 cm^{-1} in Figure 5c, indicates that cytochrome *b* remains ferric after treatment with cyanide. Table 2 illustrates that the vibrations of heme *b* obtained with the 413.1-nm laser line are essentially unchanged from those observed in spectra of the native enzyme and indicate no large changes in the coordination sphere of cytochrome *b*. Small changes in the protein constraints upon the low-spin heme *b* are suggested by the EPR *g* values which change from $g \sim 3.08$ and 1.40 to $g \sim 3.12$ and 1.34 when the enzyme is incubated in cyanide (Surerus et al., 1992).

The spectrum obtained in resonance with the cytochrome a_3 chromophore (438.2-nm excitation, Figure 5a) is best interpreted as arising from a ferrous 6cls heme A derivative. This is deduced by comparison of the 1592-cm^{-1} ν_2 and 1491-cm^{-1} ν_3 frequencies we obtain for ba_3 from Figure 5 (see Table 3) with those of the bisimidazole Fe^{2+}PA model (Table 4, column 3).

Despite the relatively poor resonance conditions, the spectrum obtained with 413.1-nm excitation in Figure 5c contains several contributions from the low-spin reduced a_3 center, as evidenced by the features at 1356, 1492(w), and 1657 cm^{-1}. The greater persistence of the a_3^{2+} features under 413.1-nm excitation in the spectra of the one-electron-reduced cyanide complex compared to that of the fully reduced, unligated complex illustrates possibly a stronger O-1 resonance enhancement mechanism (Babcock et al., 1981) and the stronger scattering of the *low-spin* heme a_3^{2+} than of the *high-spin* heme a_3^{2+} that is typical of heme RR scattering in general.

Three-Electron-Reduced (Fe_{a3}^{2+}–CN^-, Cu_B^{2+}–CN^-, Fe_a^{2+}, Cu_A^+) and Fully Reduced Cyanide Complexes. Treatment of the one-electron-reduced cyanide complex with excess sodium dithionite results in a three-electron-reduced derivative rather than a four-electron-reduced derivative. Our EPR measurements of this complex reveal that, while Cu_A is reduced, surprisingly, Cu_B remains oxidized. Figure 6a displays the EPR spectrum of the one-electron-reduced cyanide complex, and Figure 6b is that of the three-electron-reduced cyanide derivative. EPR signals attributed to both Cu_A^{2+} and Cu_B^{2+} are present in Figure 6a, as is discussed in detail in our earlier work (Surerus et al., 1992). No contributions from Cu_A^{2+} are present in Figure 6b, indicating its reduction to Cu_A^+ in this derivative. Thus, the spectrum in Figure 6b represents the EPR signal of Cu_B^{2+} obtained without interference from other metal centers and is without precedent in this regard. Figure 6b is very similar, albeit of higher quality than that obtained earlier (Surerus et al., 1992) by subtraction of the resting enzyme spectrum from that of the one-electron-reduced cyano complex, a procedure which removed contributions from Cu_A^{2+}. The similarity of the present result to that of Surerus et al. (1992) indicates that variation of the redox state of the heme *a* and Cu_A cofactors little disturbs the coordination sphere of Cu_B^{2+}. We suggest that Cu_B^{2+} remains in a strong tetragonal field that stabilizes the cupric state of this metal making it non-dithionite reducible (Surerus et al., 1992); however, other explanations are possible.

Figure 7a and b present RR spectra of this three-electron-reduced cyanide species. Reduction of cytochrome *b* to a ferrous derivative is indicated by the absence of the 1370-cm^{-1} ν_4 mode in the 413.1-nm Raman spectrum (Figure 7b) and the occurrence of a single band at 1490 cm^{-1} attributable to overlapping ν_3 vibrations from both hemes (now ferrous, 6cls). This is in contrast to the one-electron-reduced derivative which exhibits distinct ν_4 frequencies of 1356 cm^{-1} (heme a_3) and 1370 cm^{-1} (heme *b*) and ν_3 frequencies at 1492 cm^{-1} (heme a_3) and 1502 cm^{-1} (heme *b*) as shown by Figure 5c. The reduction of heme *b* is also evident from the distinctive visible bands at 530 and 560 nm characteristic of ferrous cytochrome *b* in the optical absorption spectrum of this derivative (Figure 2b).

While addition of cyanide followed by reduction with dithionite affords the three-electron-reduced cyano complex described above, addition of dithionite *first*, followed by addition of cyanide, results in a fully reduced, EPR silent species. The absence of an EPR signal attributable to Cu_B^{2+} indicates that this metal center is in its reduced state. The high-frequency RR spectrum of this fully reduced cyanide complex appears in Figure 7c. The similarity of the Raman frequencies obtained with excitation near 440 nm of the one-electron-reduced, the three-electron-reduced and the fully reduced cyanide complexes (cf., Figures 5a, 7a and 7c) attest to little change at the 6cls ferrous a_3 site resulting from the reduction of any of the other three metal centers, and the vibrational assignments in the 1150–1700-cm^{-1} range that appear in Table 3 may be taken to apply to all three complexes.

Although the vibrational *frequencies* attributed to a_3 in each of the cyanide adducts are essentially indistinguishable, subtle differences in the *relative intensities* of some of the high-frequency RR bands of the individual species are apparent (Figures 5a and 7a,c). These arise from both the slightly different excitation wavelengths employed and from a slight (~0.5 nm, see Figure 2b,c) blue-shift in the a_3 Soret absorption maximum of the four-electron-reduced cyanide derivative vs that of the three-electron-reduced species. A definite red-shift of the α band maximum of this ferrous cyanide a_3 complex occurs as each of the remaining metal centers is reduced (see Figure 2 and Table 1). That the Raman frequencies remain unchanged suggests that the ground state structure of a_3^{2+}–CN^- is constant and not affected by the redox levels of the other metals. The slight variation in the optical absorption properties most likely arises from subtle changes in the energy of the excited electronic state of the a_3 complex, perhaps due to point charge effects caused by changes in the oxidation states of the other metals, particularly Cu_B, or to protein conformational changes that accompany changes in the redox states of the metals. In addition, reduction of Cu_B results in very small (<1 nm) red-shifts in the cytochrome *b* α-band and Soret. It is unlikely that these are point charge effects of Cu_B because of the distances involved. Instead, conformational effects upon *b* of Cu_B reduction are probably responsible for these small shifts [see also Goldbeck et al. (1992)]. Finally, there are positive difference features (see difference spectrum Figure 2) at approximately 465 and 545 nm which may be due to absorptions of Cu_B^{2+} which are missing in the fully reduced derivative. Similar absorptions for Cu_B^{2+} have been suggested to appear at 390 and 520 nm for the bovine enzyme (Einarsdóttir et al., 1992).

Low-Frequency RR Measurements. Raman signals in the 150–650-cm^{-1} range of hemes include not only vibrations of the porphyrin macrocycle but also Fe-ligand motions along

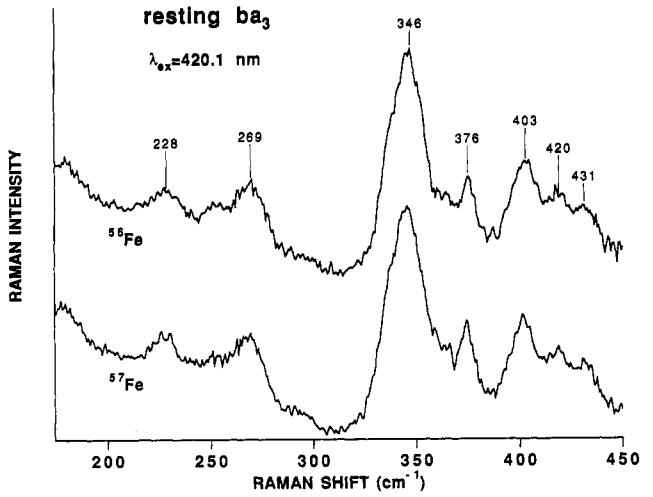

FIGURE 8: Low-frequency RR spectra of resting cytochrome ba_3 oxidase, (a) natural abundance in ^{56}Fe and (b) enriched to 95% in ^{57}Fe. Laser power at 420.1 nm was 20 mW. Samples (300 μM) were in spinning NMR tubes, at 10 °C, with 135° back-scattering geometry. Total accumulation time for each spectrum was 40 min using CCD detection and a 2400 grooves/mm grating.

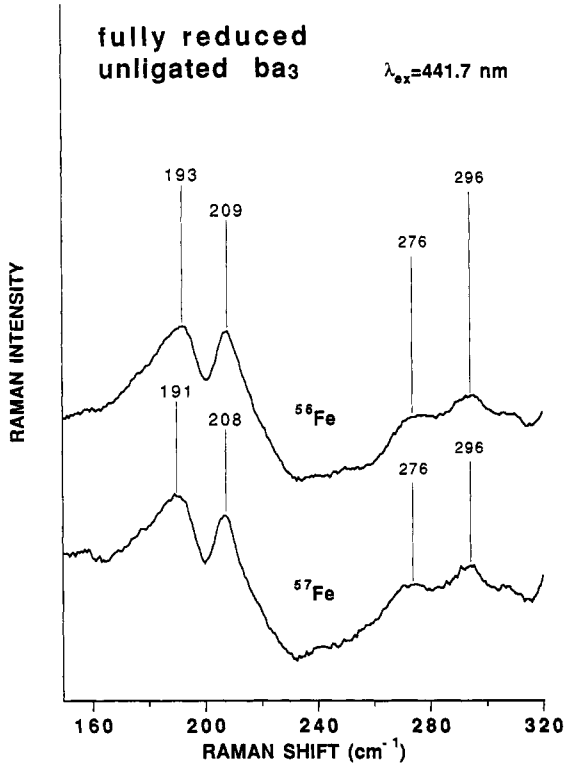

FIGURE 9: Low-frequency RR spectra of fully reduced, unligated cytochrome ba_3 oxidase, (a) natural abundance in ^{56}Fe and (b) enriched to 95% in ^{57}Fe. Laser power at 441.7 nm was 45 mW. Samples (120 μM) were in anaerobic quartz cuvettes, at 10 °C, with 135° back-scattering geometry. Total accumulation time for each spectrum was 120 min using CCD detection and a 2400 grooves/mm grating.

the axis normal to the heme plane. Because physiological function involves changes in axial ligation of Fe_{a3}, the identification and analysis of Fe–axial ligand vibrational frequencies is paramount. To facilitate such assignments, we have investigated this spectral region utilizing isotopologous varied ligands. Figures 8 and 9 show low-frequency spectra of resting and four-electron-reduced, unligated enzyme, for both natural abundance and Fe-57 enriched samples. Figure 10 displays low-frequency survey spectra at different excitation wavelengths which we use to assign porphyrin vibrations. Our

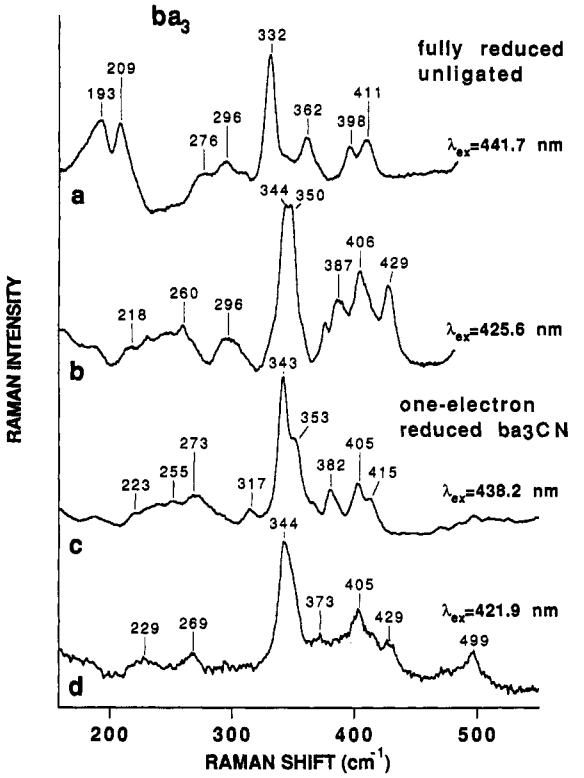

FIGURE 10: Low-frequency RR spectra of the fully reduced unligated and one-electron-reduced cyanide derivatives of cytochrome ba_3 oxidase. Spectra were collected using 135° back-scattering geometry. (a and b) Laser power at 441.7 and 425.6 nm was 45 mW. Samples (120 μM) were in anaerobic quartz cuvette, at 10 °C. Total accumulation time for spectrum a was 120 min and for spectrum b was 40 min using CCD detection and a 2400 grooves/mm grating. (c and d) Laser power at 438.2 and 421.9 nm was 30 and 18 mW, repectively. The sample (80 μM) was in a spinning NMR tube, at 10 °C. Total accumulation time for spectra c and d was 30 min each using CCD detection and a 1800 grooves/mm grating.

cytochrome a_3 vibrational assignments for this frequency region appear in Table 5 along with analogous assignments for the bovine enzyme, and, in Table 6, for heme A model compounds. Finally, low-frequency spectra of the three-electron-reduced ba_3 cyano complex for each of the four cyanide isotopomers are presented in Figure 11.

Resting and Fully Reduced Unligated ^{56}Fe and ^{57}Fe Enzyme: Detection of Two νFe_{a3}^{2+}–N(Histidine) Modes. Kitagawa and co-workers used low-frequency resonance Raman studies of fully reduced unligated derivatives of caa_3 oxidase isolated from *T. thermophilus* HB8 grown on both natural abundance ^{56}Fe and ^{54}Fe-enriched media to identify an iron–axial ligand stretching frequency at 210 cm^{-1} (Ogura et al., 1983). Given the earlier identification of a proximal histidine ligand to Fe_{a3} in this oxidase (Stevens & Chan, 1981) and work with other heme proteins and model compounds, Kitagawa's group established that this was the Fe_{a3}^{2+}–N(histidine) stretching frequency [see Kitagawa (1988) for a review]. Salmeen et al. (1978) earlier reported a similar band at 214 cm^{-1} in RR spectra of the fully reduced bovine enzyme but, because of the difficulty of isotopic substitution in the cofactors of this eucarytotic enzyme, lacked the isotope shift necessary to prove their assignment of the feature as the iron–histidine stretch.

Figure 8 displays spectra of resting ba_3 enzyme with natural abundance $^{56}Fe^{3+}$ and that enriched with $^{57}Fe^{3+}$. The Raman spectra obtained with 420.1-nm excitation of the ^{56}Fe and ^{57}Fe samples exhibit no noticeable differences indicating that there is no significant resonance enhancement of Fe^{3+}–ligand

Table 5: RR Frequencies (150–450 cm^{-1}) for Cytochrome ba_3 and aa_3 Oxidases

	ba_3			aa_3		
assignment[a]	resting 6cls a_3^{3+}	fully reduced unligated 5chs a_3^{2+}	cyanide 6cls a_3^{2+}	resting[b] 6chs a_3^{3+}	fully[c] reduced unligated 5chs a_3^{2+}	fully[c] reduced cyanide 6cls a_3^{2+}
	431					~440
$\delta C_bC_\alpha C_\beta$	420*	411	415	418	~402*	~420
	403	398	405	404	393	407
	376		382	373*		378
γ_6 pyr tilt		362*	353*		365	361
$\nu_8(\delta C_bS, \gamma C_bS)$	346*	332	343	337	327	343
$\nu_{17}(\delta C_bS)$		306 wk[d]	317		311 wk	~315
$\nu_9(\delta C_bS, \gamma C_bS)$		296				
$\nu_{52}(\delta C_bS, \nu FeN)$	269	276	271	265	279	~280
γ_{23} pyr tilt	253					
$\gamma_{24}(C_aC_m)$	228		~230	223		244*
$\nu_{34}(C_aC_b)$			~190			208
νFeN(His)		209, 193*			214	

[a] Normal mode assignments are taken from Choi and Spiro (1983), Li et al. (1989), and Li et al. (1990). [b] Taken from Schoonover et al. (1988) and Woodruff et al. (1981). Assignments for the resting forms of both oxidases are less certain due to the overlap of bands from the two hemes present. [c] Taken from Ching et al. (1985). [d] wk, weak intensity; assignment and frequency are tenative.

Table 6: RR Frequencies (150–450 cm^{-1}) for Heme A Model Compounds

assignment[a]	$(DMSO)_2Fe^{3+}PA$[b] 6chs	$(2MI)Fe^{2+}PA$[c] 5chs	$(NMI)_2Fe^{2+}PA$[d] 6cls
$\delta C_bC_\alpha C_\beta$	414	413	418
	378	383	384
γ_6 pyr tilt		367	364
$\nu_8(\delta C_bS, \gamma C_bS)$	341	343	343
$\nu_9(\delta C_bS, \gamma C_bS)$		290	299
$\nu_{52}(\delta C_bS, \nu FeN)$	268	263	264
$\gamma_{24}(C_aC_m)$			232
$\nu_{34}(C_aC_b)$			203
νFeN(NMI)		209	

[a] Normal mode assignments are taken from Choi and Spiro (1983), Li et al. 91989), and Li et al. (1990). [b] Taken from Choi et al. (1983). [c] Taken from Choi et al. (1983) and Van Steelandt-Frentrup et al. (1981). [d] Taken from Choi et al. (1983). These samples in 2% Brij contain some heme O impurities as judged from the absorption spectra.

modes from either heme *b* or heme a_3 under these conditions. Thus, we have no new evidence concerning the assignment by Schoonover et al. (1988) of a low-frequency feature at 223 cm^{-1} in the spectrum (λ_{ex} = 413.1 nm) of resting bovine aa_3 as the Fe–histidine stretch of *ferric* cytochrome a_3. On the other hand, spectra of the fully reduced, unligated ferrous ^{56}Fe and ^{57}Fe derivatives, pictured in Figure 9, reveal vibrations at 193 and 209 cm^{-1} that shift upon isotopic substitution at the metal. These intrinsic frequencies, as well as the isotopic shift, agree with assignment of each band to a Fe^{2+}–N(histidine) stretching motion of cytochrome a_3; however, the 193-cm^{-1} frequency is much lower than any reported previously for a heme protein or model compound. The occurrence of two clearly resolved bands and the temperature dependence of their relative RR intensities (not shown) suggests that there are two distinct Fe_{a3}^{2+}–N(histidine) structural conformers.

Spectral Resolution of the Low-Frequency Porphyrin Vibrations. Figure 10 displays spectra of the fully reduced unligated and the one-electron-reduced cyanide enzyme. The excitation wavelengths used for Figure 10 spectra a and c match cytochrome a_3 absorptions whereas those used in spectra b and d match absorptions of cytochrome *b*. For the fully reduced enzyme the spectral separation is excellent as exemplified by the low intensity from 190 to 210 and at 332 cm^{-1} in the spectrum obtained with 425.6-nm laser irradiation (Figure 10b) and the absence of the 344/355-cm^{-1} pair in the 441.7-nm spectrum (Figure 10a). Thus, we are confident of our assignments of the low-frequency Raman features to the individual hemes of the fully reduced, unligated enzyme which appear in Table 5.

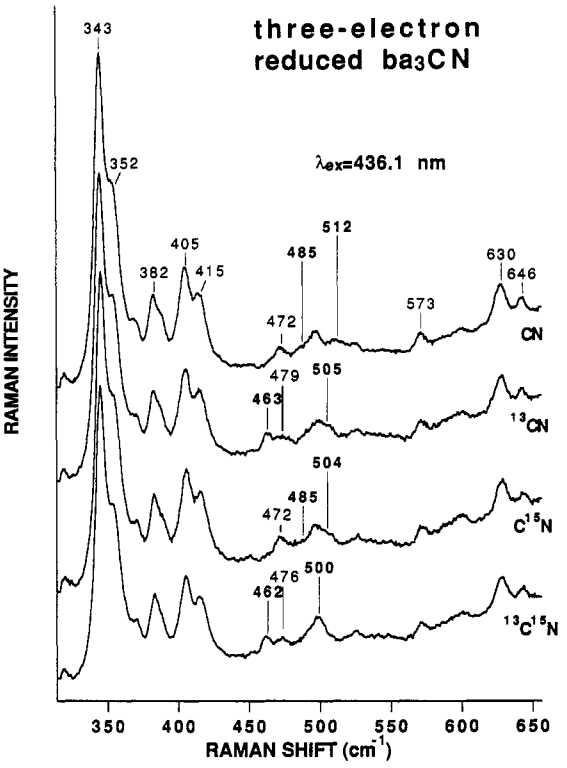

FIGURE 11: Low-frequency RR spectra of the three-electron-reduced cyanide complex of cytochrome ba_3 oxidase, (a) natural abundance in CN and (b–d) enriched to 98% in cyanide isotopomers as indicated. Laser power at 436.1 nm was 25 mW. Samples (80 μM) were in spinning NMR tubes, at 10 °C, with 135° back-scattering geometry. Total accumulation time for each spectrum was 20 min using CCD detection and a 2400 grooves/mm grating.

Because most of the features in Figure 10c have counterparts in Figure 10d, the low-frequency spectral separation afforded by selective RR excitation of the one-electron-reduced cyanide complex is more difficult to judge. It is also noteworthy that Figure 10d is very similar to the spectra in Figure 8. That is, the low-frequency spectrum obtained with excitation near 421 nm of 6cls b^{3+} and 6chs a_3^{3+} in the resting enzyme is very similar to that of the 6cls b^{3+} and 6cls a_3^{2+} moieties present in the one-electron-reduced cyano complex. This suggests that the contributions from a_3 are surprisingly weak in the *low-frequency* scattering obtained with λ_{ex} near 420 nm from

the resting enzyme and that the spectra in Figures 8 and 10d may both be dominated by vibrations of ferric cytochrome *b*. Because the contributions of b^{3+} may overlap or obscure those of a_3^{3+} in Figure 8, assignments of the resting a_3^{3+} vibrations presented in Table 5 must be considered tenative.

Fe–CN Vibrations of the Three-Electron-Reduced and Fully Reduced Cyanide Complexes. In our previous spectroscopic work on the one-electron-reduced cyanide ba_3 complex, we reported low-frequency RR spectra of four different cyanide isotopomer complexes that unambiguously established cyanide binding to a_3^{2+} via a Fe–C bond; i.e., a cyano linkage (Surerus *et al.*, 1992). We performed similar measurements for the three-electron-reduced adduct (Figure 10) and the fully reduced cyanide derivative (not shown). The results illustrate a remarkably close correspondence of the vibrational frequencies of all of these derivatives. This demonstrates that essentially no physical change occurs at the a_3 cyano binding site as a result of the sequential reduction of the other metal centers. Most importantly, the RR spectra of the fully reduced cyanide complexes obtained by addition of dithionite before cyanide (not shown) reveal no appreciable change in these Fe–CN vibrational frequencies upon reduction of Cu_B. As is the case in the high-frequency region, there are only very small differences in the low-frequency RR spectra of the one-electron-, three-electron- or fully reduced cyano complexes, and the frequencies and normal mode assignments that appear in Table 5 are considered to apply to all three.

Despite the intensive investigation of the bovine enzyme by RR, the Raman active iron–cyanide vibrations of the oxidized and partially reduced cyano complexes of this enzyme have, to date, escaped detection. We have, however, measured these vibrational frequencies for the fully reduced cyanide complex of aa_3. In collaboration with others, we have analyzed these and the analogous vibrations of the ba_3CN complexes elsewhere (Oertling et al., unpublished results). Experimentally, we find significant differences in the observed frequencies and even in the number of detectable cyanide isotope sensitive vibrations between the two oxidases. Furthermore, the geometry and force constants required to fit the data from each protein, as well as the resulting potential energy distributions of the vibrational modes, are distinct in each case, revealing significant differences in the structure and bonding of the a_3^{2+}–CN^- complexes of the two enzymes. In that work it is concluded that in cyano–ba_3 the FeCN angle is very close to 180°, whereas in reduced cyano–aa_3 the FeCN angle is approximately 170° and the Fe–C stretching force constant is significantly less than in the latter case. The structural conclusions we arrive at based on the FeCN data (Oertling et al., unpublished results) are entirely consistent with the conclusions we draw here based on the respective heme macrocycle vibrations.

DISCUSSION

Cytochrome a_3: Structural Similarities and Differences between Bacterial ba_3 and Bovine aa_3

Resting Enzyme. Room temperature RR studies on both ba_3 (see above) and bovine aa_3 (Babcock et al., 1981; Woodruff et al., 1981) indicate similar 6chs ferric a_3 configurations for the two resting enzymes. This follows from the similar ν_3 and ν_{10} frequencies (see Table 3). The ν_2 frequencies (near 1580–1590 cm^{-1}) of a_3 in the resting and cyanide adducts listed in Table 3 for the two enzymes, however, differ. This vibration has considerable $\nu(C_bC_b)$ character and thus couples to vibrations of the peripheral substituents, notably the formyl and vinyl groups, of the A type heme. In this case it is likely that the different ν_2 frequencies are caused by differences in conformations and/or electronic distributions of one or more of the peripheral substituents of the resting heme a_3 moieties in the two proteins rather than a difference in porphyrin core configurations or Fe ligation differences, as was speculated earlier (Einarsdóttir et al., 1989a). Thus, we suggest that both enzymes have a (His)N–Fe_{a3}^{3+}–X–Cu_B^{2+} configuration where a bridging ligand X couples the electron spins of the metals leaving them EPR silent.

Fully Reduced Unligated Enzyme. Our spectra indicate that Fe_{a3}^{2+} is 5chs in the reduced unligated enzyme with the proximal ligand being histidine nitrogen. The same type of structure has been established for the a_3^{2+} site in bovine oxidase (Kent et al., 1983; Stevens & Chan, 1981). Our spectra reveal two low-frequency modes which shift upon substitution of ^{57}Fe at 193 and 209 cm^{-1}. RR spectra obtained by Babcock's group of the fully reduced unliganded form of a quinol-oxidizing cytochrome aa_3 from *Bacillus subtilis* also show two bands in this region at 194 and 214 cm^{-1} (Lauraeus et al., 1993). These authors offer several interpretations of these spectral features but are tenative in their assignment of the lower frequency feature. For the fully reduced, unligated ba_3 derivative, we confidently assign both of these low-frequency bands to Fe–N(His) stretching motions because of the isotope shifts they display and the temperature dependence of their relative intensities (not shown). While details of this work will be published elsewhere (Oertling et al., unpublished results), we note that the temperature dependence of the νFe–N(His) intensities (and the thermodynamics of the conformational change inferered therefrom) is the same as that of the νFeC–O frequencies observed in our FTIR study of fully reduced *ba*–CO (Einarsdóttir et al., 1989b). The occurrence of two νFe–N(His) frequencies, with one being unusually low (Kitagawa, 1988; Smulevich et al., 1991), indicates unique structural features associated with the proximal ligation of a_3^{2+} in this enzyme which could be critical to function. With the exception of the νFe–N(His) vibration, the *overall* appearance of our spectra obtained at 441.7-nm excitation of the fully reduced unligated ba_3 (Figures 3a and 9a) is similar to the spectrum obtained by Ching et al. (1985) for bovine a_3^{2+}, also clearly 5chs, via subtraction of the cytochrome a^{2+} contribution (this basic similarity does not hold, however, for other derivatives). The agreement of the ν_2 (1579 cm^{-1}, Table 3) and ν_8 frequencies (near 330 cm^{-1}, Table 5) is particularly impressive as these are not recognizable in unsubtracted spectra of fully reduced, unligated aa_3, and this confirms the reliability of both ours and the techniques of Ching et al. (1985) to resolve spectral contributions of the individual hemes. The ~330-cm^{-1} ν_8 frequency is noteworthy as it is unique to these 5chs a_3 complexes; all other a_3 derivatives and all model complexes (including the 5chs model; see Table 6) typically display ν_8 frequencies greater than 340 cm^{-1}. This suggests a shared structural feature, presumably associated with the peripheral substituents (see below), unique to the 5chs a_3 complexes in these fully reduced, unligated cytochrome oxidases.

While our spectra and those of Ching et al. (1985) reveal a *basic* similarity between the fully reduced, unligated enzymes and shared features not found in model compounds, closer inspection of the data shows more subtle, but important differences in some of the vibrational frequencies of these 5chs a_3^{2+} complexes. In the high-frequency region, although the ν_2 frequencies of the two enzymes are identical, the $\nu_{C=O}$(formyl) frequency is higher and the $\nu_{C=C}$(vinyl) frequency is lower by 4 cm^{-1} in the bacterial compared to the mammalian complexes. Dramatically different are the ν_{11} and, to a lesser

extent, the ν_{38} and $\delta_s = CH_2(1)$ frequencies. Indeed, even the ν_8 frequencies, which are similar in their deviation from those of other a_3 derivatives and those of the model compound, differ by 5 cm^{-1}. Other low-frequency features that differ in the data are noted in Table 5. These differences most likely reflect differences in the disposition of the peripheral substituents of heme a_3 in these fully reduced unligated adducts as discussed below.

We again emphasize that there is no noticable variation in the $\nu_{10}(C_aC_m)$ core-size marker frequency ($\sim$1605–1607 cm^{-1}) in either of the a_3^{2+} adducts or the model compound. Thus, species specific structural variations in the a_3 center are most likely localized in the peripheral or the axial histidine groups rather than in core-size differences or deformations (for example, doming) of the porphyrin A moieties. This appears true for all derivatives studied.

Ferrous Cyano Complexes. Our earlier data (Surerus et al., 1992) unequivocally demonstrate cyano binding to both a_3^{2+} and Cu_B^{2+} in the mixed valence ba_3. The present study shows that reduction of the other metal centers does not significantly affect the ground state a_3^{2+}–CN^- structure, as evidenced by the absence of differences in RR frequencies of the one-, three-, and four-electron-reduced cyano derivatives (Figures 5 and 7). However, the electronic distribution in the excited state may be perturbed, as evidenced most clearly by the optical absorption difference spectrum in Figure 2. It is particularly significant that the valence of Cu_B does not appear to have a great effect on the Fe_{a3}–CN^- structure because Cu_B and heme a_3 are in close proximity to one another, coupled in their functional attributes and interactive with respect to their ligation (Palmer et al., 1976; Fiamingo et al., 1982; Scott, 1989; Woodruff et al., 1991). An IR study by Yoshikawa and Caughey (1990) indicates an a_3^{2+}–CN^-/Cu_B^{1+}–CN^- configuration for the fully reduced cyanide derivative of the bovine enzyme. All of these results indicate significant spectroscopic similarity between the bovine and bacterial enzymes, despite their considerable chemical differences (vide infra). However, comparison of the RR spectra attributed to the a_3^{2+}–CN^- chromophore of the bovine enzyme to those of the a_3^{2+}–CN^- derivatives of ba_3 may be expected to provide a sensitive measure of the detailed structural differences between the O_2 binding sites that may account for the differences in reactivity.

Inspection of Tables 3 and 5 reveals that the a_3^{2+}–CN^- complexes of bacterial ba_3 and mammalian aa_3 have distinct RR frequencies. In particular the ν_2 (1592 and 1580 cm^{-1}, respectively) and $\nu_{C=O}$(formyl) frequencies (1657 and 1644 cm^{-1}, respectively) differ greatly. Compared to the frequencies obtained from model compounds (Table 4), the ν_2 frequency for ba_3 is slightly high while the frequency of bovine aa_3 is very low. Similarly, the formyl stretching frequency for the bacterial complex is uniquely high and that of bovine aa_3 is the same as the model. Furthermore, there are a number of normal modes displaying similar frequencies in the two enzymes that are significantly different from those of the analogous model compounds, as noted in the tables. Thus, although the RR frequencies attest to basic ligation and spin state similarities in analogous ferrous heme a_3 derivatives, some stuctural differences specific the periphery of the heme a_3 moieties are evidenced by comparative RR study; particularly obvious are differences in proximal histidine ligation in fully reduced unligated adducts and formyl substituent disposition upon distal ligation of a_3^{2+} by cyanide.

A critical estimation of the nature of these structural similarities and differences between the cytochrome a_3 sites in the two proteins is revealed by inspection of the tables. In Tables 3 and 5, frequencies marked by an asterisk are those that differ significantly (by $\geq$4 cm^{-1}) in the two oxidases. This entry also differs significantly from that obtained from the appropriate model compound in solution (Table 4 and 6). Underlined entries indicate *similar* frequencies in the *two proteins* that differ significantly from those of the models. Notice that almost without exception the normal modes of note are associated with motions of the outer pyrrole C_b atoms and the peripheral substituents. This suggests that the protein matrix has substantial influence on the disposition of the peripheral substituents (most importantly the formyl, vinyl, and perhaps the farnesyl chain) in the two oxidases and that these assume unique conformations or interactions with the protein which may differ not only from one another but also from those of model compounds in solution.

Thus, our comparative structural picture of the a_3 sites in the two enzymes is as follows: in the resting oxidized forms the central Fe atoms have similar coordination properties, but there are protein effects which impose conformational differences in the peripheral substituents of the hemes. In the fully reduced, unligated derivatives, while the porphyrin A core configurations for the two enzymes are similar, there exist variations in the proximal histidine–Fe interaction and the porphyrin periphery which give rise to distinct vibrational frequencies, most notably resulting in a pair of Fe–N(His) stretching frequencies in the ba_3 data. This suggests two distinct conformers for fully reduced unligated ba_3. Finally, the ferrous cyanide complexes of both proteins most likely display distinct peripheral and proximal ligand interactions and different CN^- binding geometries as discussed elsewhere (Oertling et al., unpublished results).

Chemical Differences Between ba_3 and aa_3: Effect of the Proposed Structural Variations on the Overall Reaction of the Enzymes with Cyanide

We have shown that the reaction of the a_3/Cu_B site of resting ba_3 oxidase with cyanide can be depicted by:

$$Fe^{3+}\text{–X–}Cu^{2+} + CN^- \text{ (excess)} \rightarrow Fe^{2+}\text{–}CN^-/Cu^{2+}\text{–}CN^-$$

Autoreduction of Fe_{a3} is clear from the high-frequency RR spectrum and an absence of a bridging interaction of the cyano ligand on this metal is established by the independence of the Fe–CN vibrational frequencies on the oxidation state of Cu_B. Utilizing vibrational calculations, these latter topics are discussed in detail by Oertling et al. (unpublished results). In contrast, a considerable amount of evidence shows that the product of the reaction of cyanide with resting *bovine* oxidase is a bridged species: Fe^{3+}–CN^-–Cu^{2+} [Van Buuren et al., 1972; Thomson et al., 1981; Kent et al., 1983; Boelens et al., 1983; Li & Palmer, 1993; for a recent review, see Fee et al. (1993)]. Thus, in this case, the Fe_{a3} remains oxidized, and exchange coupling resulting from a bridging ligand most likely accounts for the absence of an EPR signal from Cu_B^{2+}. Thus, the chemical reactivity of the resting enzymes with cyanide is quite different, as is the structure of the products, and we speculate briefly on possible reasons for this.

We suggest that, in the case of ba_3, the autoreduction of the heme a_3 iron reflects an increased Fe^{3+}/Fe^{2+} reduction midpoint potential for a_3 brought about by a combination of porphyrin peripheral substituent and proximal ligand effects. The presence of electron-withdrawing substituents like the formyl and vinyl groups is known to increase the reduction potential of the central Fe (Chang et al., 1983), and these

effects are maximal when the group is restricted to a parallel configuration with respect to the heme plane (Seybert et al., 1977; Balke et al., 1985; Reid et al., 1986). That is, such electron-withdrawing, peripheral substituent effects tend to thermodynamically stabilize the ferrous over the ferric state (Balke et al., 1985, and references therein). Thus, we speculate that one or both of these substituents is in a more planar conformation in ba_3 compared to aa_3 oxidase or that the protein enhances the electron-withdrawing character of the group in some other fashion. In particular, the data in Table 3 are consistent with differences in formyl–protein interactions in cyanide derivatives of the two enzymes.

Although the formyl C=O stretching frequencies of the resting a_3^{3+} components in the two oxidases are similar (1676 cm^{-1}), the $\nu_{C=O}$(formyl) frequency of the a_3^{2+} cyano adduct is not depressed in the ba_3 species (1657 cm^{-1}) to the extent that it is in bovine aa_3 or the ferrous cyano porphyrin A model compounds (1644 cm^{-1}; see Tables 3 and 4). We also note that the vinyl ν(C=C) frequency appears slightly lower in the bacterial than in the mammalian enzyme. That is, the splitting between these frequencies is largest for cyano ba_3. Thus, in the bacterial enzyme, ligation of the Fe_{a3} and Cu_B metal centers appears to trigger a change in the vinyl and or formyl configurations which stabilizes the ferrous state of a_3. Logically, this might correspond to conformations more coplanar to the heme plane for each. This would not only maximize the extent to which the peripheral substituents could modulate the reduction potential but also may maximize coupling between the two vibrations and drive the frequencies in the directions observed. This ligation-dependent protein influence on the peripheral substituents is also expected to affect the frequencies of other vibrations which are coupled to the $\nu_{C=O}$(formyl) motion, such as the high-frequency ν-(C_bC_b) modes, ν_2, ν_{11}, and ν_{38} (Willems & Bocian, 1984), and various low frequency vibrations, for example, the vinyl-related mode at 410–420 cm^{-1}. Thus, if the different redox chemistry of a_3 in the two proteins is caused by different formyl and vinyl configurations, we expect frequency differences in these vibrations, as is observed (see tables).

Analysis of cytochrome a_3 formyl stretching frequencies is complicated by a number of factors. In porphyrin A complexes of iron the $\nu_{C=O}$(formyl) is modulated by the central metal by virtue or the $Fe_{d\pi}$–porphyrin$_{\pi^*}$ orbital overlap. The formyl frequency is lowered for ferrous compared to ferric complexes in a manner similar to the ν_4(C_aN) mode (the "oxidation state marker"). That is, electron donation by the metal into the porphyrin π^* orbital can lower both frequencies. Thus, the formyl C=O stretch of ferrous heme A is dependent on anything that modulates this metal to porphyrin electron donation: iron coordination number (5 or 6), solvent, or the π acceptor/donor properties of the axial ligands [for review, see Babcock (1988)]. Furthermore, a reliable correlation of the frequencies of these two modes, ν_4 and $\nu_{C=O}$(formyl), is not apparent from the existing data. Thus, in addition to geometric and kinematic effects, electronic effects that will change vibrational force constants are expected to modulate the $\nu_{C=O}$(formyl) frequency.

A first step toward more specific correlation of vinyl and formyl conformations to the observed frequencies is a more detailed analysis of the normal modes involving the peripheral groups of heme A. We emphasize that normal mode calculations on heme A or any *trans*-vinyl, formyl porphyrin complex do not exist in the literature. The calculations upon which our vibrational assignments are based are ultimately for more symmetrical metalloporphyrins (Abe, et al., 1978; Li et al., 1989, 1990) with different peripheral substituents. It is thus of little use to speculate further the geometries of the various heme A peripheral groups to which the observed frequencies correspond without a more detailed description of the specific normal modes of heme A. What seems clear from our data, however, is that there are differences in the disposition of these groups among the cytochrome a_3 and model complexes here discussed, and this has long been suggested to be a very viable mechanism for protein control of heme redox chemistry (Chang et al., 1983; Reid et al., 1986).

Another plausible contributing factor to the autoreduction of the a_3 iron in the bacterial oxidase could be the unique proximal imidazole interaction suggested by the νFe–N(His) frequencies in the reduced unligated protein. It is known that heme peroxidases display lowered reduction potentials and have relatively high νFe–N(His) frequencies $\sim$240 cm^{-1} (Morrison & Schonbaum, 1976; Teraoka & Kitagawa, 1981; Smulevich et al., 1991). Thus it is reasonable that the relatively low νFe–N(His) frequencies of ba_3 could reflect protein control that tends to *raise* the Fe_{a3} redox potential via a proximal ligand effect. Paul et al. (1985a) have calculated the heme Fe^{3+}/Fe^{2+} redox potential as a function of the Fe–N(His) distance and confirm a sight dependence but suggest that the primary mechanism by which the protein matrix modulates the heme redox potential in the peroxidases arises from interactions of the distal arginine residue present in the pocket with the porphyrin ring, rather than from proximal effects imposed by the fifth ligand, histidine.

Thus, our chemical model of the a_3 site in the bacterial enzyme is of a heme complex in which the ferrous state is stabilized over the ferric in the presence of cyanide. This presumably reflects a ferrous heme in which the Fe^{2+} center is stabilized by electron density withdrawal. This condition is most likely caused by peripheral or possibly proximal effects that are absent or less effective in the mammalian cytochrome a_3 site. The ferrous center in complexes with other ligands may be electron poor as well; we note that the νCO frequency of the carbon monoxy complex of ba_3 (1983 cm^{-1}) is much higher than the corresponding frequency in CO complexes of aa_3 [1963 cm^{-1}; see Einarsdóttir et al. (1989b) and references therein]. This is consistent with correlations of Fe reduction potential with νCO of ferrous carbonyl porphyrins compiled by Paul et al. (1985b). The highest νCO value these authors report (1980 cm^{-1}) is for a 2,4-diformyl heme, for which they extrapolate their correlation to speculate a redox potential of approximately 390 mV. In this model compound, the two electron-withdrawing formyl groups most likely raise the iron redox potential and cause the high νCO. Thus, this study is fully consitent with our interpretation of the ba_3 data. The higher νCO value for the bacterial enzyme suggests weaker $Fe_{d\pi}$ CO$_{\pi^*}$ back-bonding in the ba_3 than in the aa_3 complex, consistent with less electron density at the Fe in the case of ba_3.

Cu_B

Although the silent partner in the resonance Raman experiment, the role of Cu_B in the ligand binding site of cytochrome oxidases is being revealed in the case of CO binding to the mammalian enzyme (Dyer et al., 1989, 1991; Woodruff et al., 1991). Details of the kinetics and thermodynamics of CO binding and rebinding under photolysis conditions for the different oxidase enzymes have been compared (Einarsdóttir et al., 1989b, 1993; D. D. Lemon et al., unpublished results). There are evident chemical differences between cytochrome

ba_3 and other heme–copper oxidases, in addition to the cyanide chemistry discussed previously. For example, the equilibrium constant for CO binding to Cu_B^+ is approximately 100 times greater for ba_3 than for bovine aa_3, and the kinetics of the subsequent transfer of CO from Cu_B^+ to Fe_{a3}^{2+} also differ in the two enzymes (D. D. Lemon et al., unpublished results). The differences in ligand binding behavior that these studies reveal undoubtedly result from structural variations at the binuclear heme/Cu pair. The fact that Cu_B in ba_3 appears able to assume well-defined tetragonal coordination to four approximately equivalent histidine nitrogens is clear evidence for structural differences. We have speculated elsewhere that the nearly conserved histidine residue in the loop between helices IX and X provide the fourth imidazole ligand in the cyano-ba_3 complex (Fee et al., 1993; Keightley, 1993). Cu_B in bovine cytochrome aa_3 is apparently unable to adopt such a ligand configuration.

ACKNOWLEDGMENT

W.A.O. thanks Drs. R. Donohoe, M. Tecklenburg, R. Wever, and J. Babcock for helpful discussions.

REFERENCES

Abe, M., Kitagawa, T., & Kyogoku, Y. (1978) *J. Chem. Phys. 69*, 4526–4534.

Argade, P. V., Ching, Y.-C., & Rousseau, D. L. (1986) *Biophys. J. 50*, 613–620.

Babcock, G. T. (1988) in *Biological Applications of Raman Spectroscopy* (Spiro, T. G., Ed.) Vol. 3, pp 294–346, John Wiley & Sons, Inc., New York.

Babcock, G. T., & Callahan, P. M. (1983) *Biochemistry 22*, 2314–2318.

Babcock, G. T., & Wikström, M. (1992) *Nature 356*, 301–309.

Babcock, G. T., Callahan, P. M., Ondrias, M. R., & Salmeen, I. (1981) *Biochemistry 20*, 959–966.

Babcock, G. T., Widger, W. R., Cramer, W. A., Oertling, W. A., & Metz, J. G. (1985) *Biochemistry 24*, 3638–3645.

Baker, G. M., Noguchi, M., & Palmer, G. (1987) *J. Biol. Chem. 262*, 595–604.

Balke, V. L., Walker, F. A., & West, J. T. (1985) *J. Am. Chem. Soc. 107*, 1226–1233.

Boelens, R., Wever, R., Van Gelder, B. F., & Rademaker, H. (1983) *Biochim. Biophys. Acta 724*, 176–183.

Boelens, R., Rademaker, H., Wever, R., & Van Gelder, B. F. (1984) *Biochim. Biophys. Acta 765*, 196–209.

Brudvig, G. W., Stevens, T. H., Morse, R. H., & Chan, S. I. (1981) *Biochemistry 20*, 3912–3921.

Callahan, P. M., & Babcock, G. T. (1981) *Biochemistry 20*, 952–958.

Callahan, P. M., & Babcock, G. T. (1983) *Biochemistry 22*, 452–461.

Capapldi, R. A. (1990) *Annu. Rev. Biochem. 59*, 569–596.

Carter, K. R., Antalis, T. M., Palmer, G., Ferris, N. S., & Woodruff, W. H. (1981) *Proc. Natl.. Acad. Sci. U.S.A. 78*, 1652–1655.

Chan, S. I., & Li, P. M. (1990) *Biochemistry 29*, 1–12.

Chang, C. K., Hatada, M. H., & Tulinsky, A. (1983) *J. Chem. Soc., Perkin Trans II*, 371–378.

Ching, Y.-C., Argade, P. V., & Rousseau, D. L. (1985) *Biochemistry 24*, 4938–4946.

Choi, S., Spiro, T. G., Langry, K. C., Smith, K. M., Budd, D. L., & La Mar, G. N. (1982) *J. Am. Chem. Soc. 104*, 4345–4351.

Choi, S., Lee, J. J. Wei, Y. H., & Spiro, T. G. (1983) *J. Am. Chem. Soc. 105*, 3692–3707.

Cline, J., Reinhammar, B., Jensen, P., Venters, R., & Hoffman, B. M. (1983) *J. Biol. Chem. 258*, 5124–5128.

Curtis, Y. M., & Curtis, N. F. (1966) *Aust. J. Chem. 19*, 609–616.

Dyer, R. B., Einarsdottir, O., Killough, P. M., Lopez-Garriga, J. J., & Woodruff, W. H. (1989) *J. Am. Chem. Soc. 111*, 7657–7659.

Dyer, R. B., Peterson, K. A., Stoutland, P. O., & Woodruff, W. H. (1991) *J. Am. Chem. Soc. 113*, 6276–6277.

Einarsdóttir, Ó., Choc, M. G., Weldon, S., & Caughey, W. S. (1988) *J. Biol. Chem. 263*, 13641–13654.

Einarsdóttir, Ó., Dyer, R. B., Killough, P. M., Fee, J. A., & Woodruff, W. H. (1989a) *Proc. SPIE—Int. Soc. Opt. Eng. 1055*, 254–262.

Einarsdóttir, Ó., Killough, P. M., Fee, J. A., & Woodruff, W. H. (1989b) *J. Biol. Chem. 264*, 2405–2408.

Einarsdóttir, Ó., Dawes, T. D., & Georgiadis, K. E. (1992) *Proc. Natl. Acad. Sci. U.S.A. 89*, 6934–6937.

Einarsdóttir, Ó., Dyer, R. B., Lemon, D. D., Killough, P. M., Hubig, S. M., Atherton, S. F., López-Garriga, J. J., Palmer, G., & Woodruff, W. H. (1993) *Biochemistry 32*, 12013–12024.

Fee, J. A., Yoshida, T., Surerus, K. K., & Mather, M. W. (1993) *J. Bioenerg. Biomembr. 25*, 103–114.

Goldbeck, R. A., Einarsdóttir, Ó., Dawes, T. D., O'Conner, D. B., Surerus, K. K., Fee, J. A., & Kliger, A. S. (1992) *Biochemistry 31*, 9376–9387.

Hartzell, C. R., Beinert, H., Babcock, G. T., Chan, S. I., Palmer, G., & Scott, R. A. (1988) *FEBS Letts. 236*, 1–4.

Hill, B. C., Greenwood, C., & Nicholls, P. (1986) *Biochim. Biophys. Acta 853*, 91–113.

Johnson, M. K., Eglinton, D. G., Gooding, P. E., Greenwood, C., & Thomson, A. J. (1981) *Biochem. J. 193*, 699–708.

Keightley, J. A. (1993) Ph.D. Thesis, University of New Mexico, Albuquerque.

Kent, T. A., Münck, E., Dunham, W. T., Filter, W. A., Findling K. L., Yoshida, T., & Fee, J. A. (1982) *J. Biol. Chem. 257*, 12489–12492.

Kent, T. A., Young, L. J., Palmer, G., Fee, J. A., & Munck, E. (1983) *J. Biol. Chem. 258*, 8543–8546.

Kitagawa, T. (1988) in *Biological Applications of Raman Spectroscopy* (Spiro, T. G., Ed.) Vol. 3, pp 97–132, John Wiley & Sons, Inc., New York.

Lauraeus, M., Wikstrom, M., Varotsis, C., Tecklenburg, M. J., & Babcock, G. T. (1993) *Biochemistry 31*, 10054–10060.

Li, W., & Palmer, G. (1993) *Biochemistry 32*, 1833–1843.

Li, X.-Y., Czernuszewicz, R. S., Kincaid, J. R., & Spiro, T. G. (1989) *J. Am. Chem. Soc. 111*, 7012–7023.

Li, X.-Y., Czernuszewicz, R. S., Kincaid, J. R., Stein, P., & Spiro, T. G. (1990) *J. Phys. Chem. 94*, 47–61.

López-Garriga, J. J., Oertling, W. A., Kean, R. T., Hoogland, H., Wever, R., & Babcock, G. T. (1990) *Biochemistry 29*, 9387–9395.

Ludwig, B. (1987) *FEMS Microbiol. Rev. 46*, 41–56.

Malström, B. G. (1990) *Chem. Rev. 90*, 1247–1260.

Morrison, M., & Schonbaum, G. R. (1976) *Annu. Rev. Biochem. 45*, 86–127.

Musser, S. M., Stowell, M. H. H., & Chan, S. (1993) *FEBS Lett. 327*, 131–136.

Ogura, T., Hon-nami, K., Oshima, T., Yoshikawa, S., & Kitagawa, T. (1983) *J. Am. Chem. Soc. 105*, 7781–7783.

Palmer, G., Babcock, G. T., & Vickery, L. E. (1976) *Proc. Natl. Acad. Sci. U.S.A. 73*, 2206–2210.

Paul, J., Smith, M. L., & Paul, K.-G. (1985a) *Biochim. Biophys. Acta 832*, 257–264.

Paul, J., Smith, M. L., Norden, B., & Paul, K.-G. (1985b) *Biochim. Biophys. Acta 832*, 265–273.

Powers, L., Blumber, W., Chance, B., Barlow, C., Leigh, J. S., Smith, J., Yonetani, T., Vik, S., & Peisach, J. (1979) *Biochim. Biophys. Acta 546*, 520–531.

Puettner, I., Carafoli, E., & Malatesta, F. (1985) *J. Biol. Chem. 260*, 3719–3723.

Reid, L. S., Lim, A. R., & Mauk, A. G. (1986) *J. Am. Chem. Soc. 108*, 8197–8201.

Salmeen, I., Rimai, L., & Babcock, G. T. (1978) *Biochemistry 17*, 800–806.

Saraste, M., Holm, L., Lemieux, L., & Vanderoost, J. (1991) *Biochem. Soc. Trans. 19*, 608–612.
Schoonover, J. R., Dyer, R. B., Woodruff, W. H., Baker, G. M., Noguchi, M., & Palmer, G. (1988) *Biochemistry 27*, 5433–5440.
Scott, R. A. (1989) *Annu. Rev. Biophys. Biophys. Chem. 18*, 137–158.
Scott, R. A., Schwartz, J. R., & Cramer, S. P. (1986) *Biochemistry 25*, 5546–5555.
Seybert, S. W., Moffat, K., Gibson, Q. H., & Chang, C. K. (1977) *J. Biol. Chem. 525*, 4225–4231.
Smulevich, G., Miller, M. A., Kraut, J., & Spiro, T. G. (1991) *Biochemistry 30*, 9546–9558.
Sone, N., & Fujiwara, Y. (1991) *FEBS Lett. 288*, 154–158.
Spaulding, L. D., Chang, C. C., Yu, N.-T., & Felton, R. H. (1975) *J. Am. Chem. Soc. 97*, 2517–2525.
Stevens, T. H., & Chan, S. I. (1981) *J. Biol. Chem. 256*, 1069–1071.
Surerus, K. K., Oertling, W. A., Fan, C., Gurbiel, R. J., Einarsdottir, O., Antholine, W. E., Dyer, R. B., Hoffman, B. M., Woodruff, W. H., & Fee, J. A. (1992) *Proc. Natl. Acad. Sci. U.S.A. 89*, 3195–3199.
Swanson, B. I., & Rafalko, J. J. (1976) *Inorg. Chem. 15*, 249–253.
Teraoka, J., & Kitagawa, T. (1981) *J. Biol. Chem. 256*, 3969–3977.
Thomson, A. J., Johnson, M. J., Greenwood, C., & Gooding, P. E. (1981) *Biochem. J. 193*, 687–697.
Tsubaki, M., & Yoshikawa, S. (1993) *Biochemistry 32*, 164–173.
Van Buuren, K. J. H., Nicholls, P., & Van Gelder, B. F. (1972) *Biochim. Biophys. Acta 256*, 258–276.
Vanneste, W. (1966) *Biochemistry 5*, 838–848.
Van Steelandt-Frentrup, J., Salmeen, I., & Babcock, G. T. (1981) *J. Am. Chem. Soc. 103*, 5981–5982.
Wicholas, M., & Wolford, T. (1974) *Inorg. Chem. 13*, 316–318.
Willems, D. L., & Bocian, D. F. (1984) *J. Am. Chem. Soc. 106*, 880–890.
Wilson, E. B., Jr., Decius, J. C., & Cross, P. C. (1955) in *Molecular Vibrations. The Theory of Infrared and Raman Vibrational Spectra* (originally published in 1955; updated in 1980) Dover, New York.
Woodruff, W. H., Dallinger, R. F., Antalis, T. M., & Palmer, G. (1981) *Biochemistry 20*, 1332–1338.
Woodruff, W. H., Kessler, R. J., Ferris, N. S., Dallinger, R. F., Carter, K., Antalis, T. M., Palmer, G. (1983) *Adv. Chem. Ser. 201*, 625.
Woodruff, W. H., Einarsdóttir, Ó., Dyer, R. B., Bagley, K. A., Goldbeck, R. A., Dawes, T. D., & Kliger, D. S. (1991) *Proc. Natl. Acad. Sci. U.S.A. 88*, 2588–2592.
Wu, W., Chang, C. K., Varotsis, C., Babcock, G. T., Puustinen, A., & Wikstrom, M. (1992) *J. Am. Chem. Soc. 114*, 1182–1187.
Yoshikawa, S., & Caughey, W. S. (1990) *J. Biol. Chem. 265*, 7945–7958.
Yu, N.-T., & Kerr, E. A. (1988) in *Biological Applications of Raman Spectroscopy* (Spiro, T. G., Ed.) Vol. 3, pp 39–95, John Wiley & Sons, Inc., New York.
Zimmermann, B. H. (1988) Ph.D. Thesis, University of Michigan, Ann Arbor.
Zimmermann, B. H., Nitsche, C. I., Fee, J. A., Rusnak, F., & Munck, E. (1988) *Proc. Natl. Acad. Sci. U.S.A. 85*, 5779–5783.